Improved model for air pressure due to wind on 2D freak waves in finite depth

S. Yan and Q.W. Ma*
School of Engineering and Mathematical Sciences, City University, London, EC1V 0HB, UK

Abstract

This paper presents an improved model for evaluating air pressure acting on 2D freak waves in finite depth due to the presence of winds. This pressure model is developed by analysing the pressure distribution over freak waves using the QALE-FEM/StarCD approach, which combines the quasi arbitrary Lagrangian-Eulerian finite element method (QALE-FEM) with the commercial software package StarCD and has been proven to be sufficiently accurate for such cases according to our previous publication [8]. In this model for air pressure, the pressure is decomposed into the components related to the local wave profiles and others. By coupling with the QALE-FEM, the accuracy of the pressure model is tested using various cases. The results show that the pressure distribution estimated using this model is close to that computed by using the QALE-FEM/StarCD approach when there is no significant vortex shedding and wave breaking. The accuracy investigation in predicting the freak wave heights and elevations demonstrates that this pressure model is much better than others in literature so far used for modelling wind effects on freak waves in finite depth.

Key words: Wind effects; Freak waves; air pressure; QALE-FEM; Numerical simulation

1. Introduction

Freak waves have attracted the interests of many researchers because of their real threat to human activities in the oceans although their low possibility of occurrence [1]. Observations have confirmed that such extreme wave event may occur in both shallow and deep water [2]. Effort has been devoted to get a good understanding of freak waves, e.g. their physical properties and possible generation mechanisms. Detailed reviews may be found in [2] and [3]. Although freak waves are often observed being accompanied with strong winds (e.g. [4]), related studies on freak waves under the action of winds are still limited. Generally speaking, when the wind speed is very small, its effects may be neglected; otherwise, the wind

* Corresponding author. Tel.: +44 20 7040 8159; fax: +44 20 7040 8566
E-mail address: q.ma@city.ac.uk (Q.W. Ma)

may initiate freak waves or dramatically influence the property of freak waves generated mainly by other mechanisms. So far, the problem regarding whether the formation of freak waves is caused by the wind has not been confirmed by experiments, but, several laboratory experiments [5-7] have demonstrated that the winds may dramatically affect 2D freak waves. This calls for a detailed investigation of freak waves under the action of winds.

The problem involved is a fully-coupled interaction between air flows and freak waves. To study this, three issues need to be addressed. The first one is the feature of the air flow during the propagation of freak waves, the second one is the mechanism of energy/momentum exchanging between the wind and the freak waves and the third one is about how the profile of the freak waves changes as the presence of winds. Considering the strong nonlinearity associated with freak waves, four numerical strategies may be implemented as summarised in [8,9]. Only the second strategy, in which a fully nonlinear potential flow (FNPT) is applied to govern the wave motion coupling with a model expressing the wind-excited pressure, and the fourth one, which combines a FNPT model with a Navier-Stokes solver, have been attempted for the cases with freak waves [8]. The former has been applied by Touboul et al. [6], Kharif et al. [7] and Touboul and Kharif [10] to simulating wind effects on 2D freak waves generated by spatio-temporal focusing and modulation instability. Using a similar model, Ma and Yan [11] preliminarily studied wind effects on 2D/3D freak waves. The latter is suggested and adopted by the authors of this paper [8,9] to simulate the interaction between winds and 2D breaking freak waves [8,11]. Compared with the former, the latter considers the viscosity, turbulence and is able to deal with breaking waves. Nevertheless, the computational efficiency is lower. Therefore, it is understandable to suggest that the second approach is preferred for the cases without breaking waves, while, the third approach is better to handle the cases with breaking waves.

The success of the FNPT model (the second strategy) in simulating freak waves under action of winds largely depends on the model to implement wind effects. For this purpose, we need to have a good understanding of the mechanism of energy/momentum exchanging between the wind and the freak waves, i.e. the second issue involved in this problem as discussed above. Some mechanisms quantifying the consequential growth rate of the waves have been suggested to explain the wave growth by the presence of winds, such as Jeffreys' sheltering mechanism [12-13], Miles' shearing mechanism [14-19], Philips' model [20], Benjamin's model [21] and other mechanisms by Belcher and Hunt [22]. However, these models are

based on the linear water wave theory. Once the wave steepness is relatively larger, the air pressure estimated using those models may be insufficiently accurate as demonstrated by Sullivan et al [23]. Therefore, for freak waves, normally involves strong nonlinearity, those models may need to be modified. For the purpose, Kharif et al [7] experimentally studied the feature of the energy/moment flux in the cases with deep-water freak waves and concluded that air flow separation occurring at the lee side of the crest is mainly responsible for the energy transfer from the winds to the freak waves, causing wave growth. According to this, they suggested a modified Jeffreys' theory to model the wind-excited free surface pressure. By adopting this model, Touboul et al [6] and Kharif et al. [7] proposed a FNPT based boundary integral equation method to simulate wind effects on 2D freak waves. Comparison between their numerical results and the experimental data confirms that by applying such simplified mechanisms, the FNPT model can achieve acceptable accuracy in many cases. Nevertheless, the numerical investigation by Yan and Ma [8] demonstrates that the modified Jeffreys' theory does not generally lead to consistent pressure distribution with those predicted by a fully-coupled NS model. This calls for a further study on the feature of the air pressure due to winds in the cases with freak waves to develop a better pressure model.

Apart from the air pressure distribution, another issue is the wind-driven current, which plays important role in shifting the focusing point as demonstrated by Giovanangeli et al [5] and Kharif et al [7]. In reality, the wind-driven current varies along the vertical direction [24]. For simplification, in the FNPT model for wave-current interaction, a constant current is usually applied (e.g. [25,26]). Although the current has been suggested to be 3% of wind speed, it does not always lead to acceptable results. A numerical investigation needs to be carried out to find a proper value of the current to ensure the overall effect of the current simulated using such simplified model is close to the reality, which has not been done to the best of our knowledge .

This paper will present systematic investigations carried out by using the QALE-FEM/StarCD approach [8] on the interaction between winds and 2D freak waves generated by the spatio-temporal focusing mechanism in finite depth. Based on the investigations, an improved model is suggested to estimate the pressure distribution on the free surface of freak waves and to give more suitable current value. The accuracy of the improve model is demonstrated in terms of both providing spatio-temporal pressure distribution and simulating the formation of freak waves.

2. Mathematical model and numerical approach

In this paper, two numerical models will be used to study the air pressure on the water surface. The first one is the QALE-FEM method based on the FNPT model. The second one is the QALE-FEM/StarCD approach combing the QALE-FEM and the commercial software package StarCD. Necessary brief is given in this section.

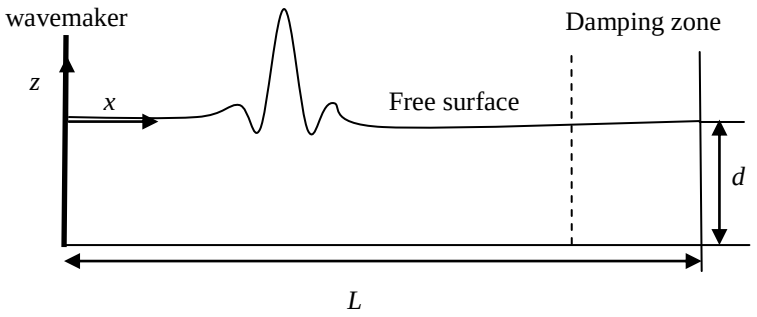

Fig. 1. Sketch of fluid domain

2.1. FNPT based QALE-FEM method

In the QALE-FEM method, the computational domain is chosen as a rectangular tank. The freak wave is generated in the tank by a piston-like wavemaker. The wavemaker is mounted at the left end and a damping zone with a Sommerfeld condition (see [27-31] for details) is applied at the right end of the tank in order to suppress the reflection, as sketched in Fig. 1 where L and d represent the total length of the tank and water depth, respectively. Winds with speed of U_w in x-direction may be introduced. A constant x-direction current may be added to model the effect of the wind-driven current. A Cartesian coordinate system is used with the ox axis on the mean free surface and with the z-axis being positive upwards. The origin of the coordinate system is located at the left end of the tank.

The total velocity potential (Φ) is expressed by

$$\Phi = \phi + U_c x, \tag{1}$$

where U_c is the current speed and ϕ is the rest of the velocity potential apart from xU_c. In the fluid domain, the velocity potential satisfies the Laplace's equation, $\nabla^2 \Phi = 0$, leading to

$$\nabla^2 \phi = 0, \tag{2}$$

On the free surface $z = \varsigma(x,t)$ where ς is the wave elevation, ϕ satisfies the kinematic and dynamic conditions in the following Lagrangian form,

$$\frac{Dx}{Dt} = \frac{\partial \phi}{\partial x} + U_c, \frac{Dz}{Dt} = \frac{\partial \phi}{\partial z}, \tag{3}$$

$$\frac{D\phi}{Dt} = -gz + \frac{1}{2}|\nabla \phi|^2 + p_{sf} - \frac{U_c^2}{2} \quad , \tag{4}$$

where $\frac{D}{Dt}$ is the substantial (or total time) derivative following fluid particles and g is the gravitational acceleration. p_{sf} is the free-surface pressure, which is taken as zero for the cases without winds [27,29]. For the cases with winds, the value of p_{sf} is estimated by using an improved model purpose-developed for freak waves or focusing wave groups. The details about this will be discussed in the following sections.

In this paper, the waves are generated by a piston-type wavemaker, on which the corresponding boundary condition of ϕ is,

$$\frac{\partial \phi}{\partial n} = \vec{n} \cdot \vec{U}(t) \ , \tag{5}$$

where $\vec{n}$ is the outward unit normal vector of the wavemaker; $\vec{U}(t)$ is its oscillating velocity, which is specified by using linear wavemaker theory [32]. For example, it may be specified as $\vec{U}(t) = a \sin \omega t / F$, where F is the wavemaker transfer function, to generate a monochromic wave with amplitude of a and frequency of ω [27].

The problem formed by Eqs. (1)-(5) is solved by the QALE-FEM method using a time-marching procedure. At each time step, the boundary value problem for the velocity potential ϕ is solved by the FEM. The details about the FEM formulation have been described in our previous publications [27-28] and will not be repeated here. The main difference between the QALE-FEM method and the conventional FEM method [28] mainly includes two aspects when they are applied to modelling wave problems without structures. One is that the computational mesh is moving in the QALE-FEM method, instead of being regenerated, at every time step during the calculation. To do so, a novel methodology has been suggested to control the motion of the nodes, in which interior nodes and nodes on the free surface (free-surface nodes) are separately considered. Different methods are employed for moving different groups of nodes. The other difference between the QALE-FEM and conventional FEM methods is the calculation of the fluid velocity on the free surface. The technique developed in the QALE-FEM is suitable for computing the velocity when waves become very steep or even overturning. More details of these techniques can be found in [27,29].

2.2. QALE-FEM/StarCD approach

In the QALE-FEM/StarCD approach, the in-house software package based on the QALE-FEM is combined with the commercial software (StarCD). The former has been briefly described above. The latter is a multi-phase module solving general Reynolds-Averaged Navier-Stokes (RANS) equations using the finite volume method. This approach can simulate wave breaking, viscosity and the wind-wave interaction.

When applying this approach, the whole spatial domain is decomposed into two sub-domains. The first one Ω_F ranges from the wavemaker to an artificial boundary Γ_I, in which the QALE-FEM method is applied and the boundary conditions are described in Eqs. (3)-(5). According to our numerical test [8], it is suitable to choose $3d$ for the length of the domain Ω_F (L_F). The second one Ω_S covers the rest part of the domain where the StarCD package is employed. In this domain, Dirichlet condition of fluid velocity and the value of the fraction function denoting the volume of fluid are specified on the inlet boundary (Γ_I), a pressure condition is imposed on the outlet boundary. On the bottom of the domain, a non-slip condition is imposed. Since the top boundary is an artificial wall, a slip condition is imposed and numerical tests are required for all cases to avoid its effect on the air flow structure and the vorticity near the free surface. Based on our numerical investigations, the height of the domain for the StarCD simulation is chosen $16d$ for all the cases presented in this paper.

During the simulation, the whole procedure is also separated into two stages. At each stage the calculation starts from $t = 0$ and stops when the required duration of simulation is achieved. In the first stage, the QALE-FEM calculation is run in a numerical tank with length of $L_F+3d+\min(3d, 3\lambda_{max})$ in which λ_{max} is the maximum wavelength of all wave components considered. The velocity and the wave elevation at $x=L_F$ (corresponding to the position of the artificial boundary Γ_I) are recorded at every time step for the purpose of providing the boundary condition for the StarCD simulation. In this stage, the modified Jeffreys' theory [6,7], which may be sufficiently accurate for relatively small waves[8], is employed to model the wind pressure. The wind-driven current in the QALE-FEM model is taken as zero, which ensures the velocity field at the inlet of the StarCD calculation does not include wind-driven current term. In the second stage, the StarCD calculation is run in the sub-domain Ω_S. On its inlet boundary (Γ_I), the fluid velocity and the value of the fraction function at each cell of the computational mesh are specified by using the fluid velocity and the wave elevation obtained from the first-stage calculation, respectively. Due to the fact that the QALE-FEM

model and the StarCD model require significantly different mesh resolution and time step (specifically $0.05d$, $0.025\sqrt{d/g}$ are required by the QALE-FEM and $0.008d$, $0.006\sqrt{d/g}$ by the StarCD, respectively, for all cases presented here) to achieve convergent results, a moving least square method is applied in the spatial domain and a second-order polynomial interpolation is employed in the time domain to specify the inlet velocity and the fraction function for the StarCD model. More details can be found in [8].

3. Improved model for air pressure and estimation of wind-driven current

As indicated in the Introduction, to model freak waves under the action of winds using the FNPT model, both the spatial-temporal distribution of the free surface pressure excited by the winds and the wind-driven current need to be considered. The methods to model these will be discussed in this section.

3.1. Free surface pressure excited by winds

Touboul et al [6] experimentally studied the amplification of the wave height along the direction of the freak wave propagating and found that the difference of the amplification factors in the cases with different wind speeds is significant only after the focusing point. They also observed that the air flow separation occurs in the lee side of a steep wave crest, which is responsible for the growth and persistence of steep waves. Therefore, they suggested using the Jeffreys' sheltering theory, to model the pressure. By adopting the Jeffreys' theory locally in time and space, Touboul et al [6] and Kharif et al [7] give the free surface pressure distribution for 2D cases as followed,

$$p_{sf} = \rho_a s U_w^{*2} \frac{\partial \varsigma}{\partial x}, \tag{6}$$

where the constant s is the sheltering coefficient. ρ_a is the atmospheric density; U_w^* is the wind speed relative to the characteristic velocity of the wave and is given by

$$U_w^* = U_w - c \tag{7}$$

in which U_w and c are the wind speed and the wave phase velocity. Considering that this mechanism is applicable only if the waves are sufficiently steep to produce an air flow separation, the model is modified by introducing a threshold value for the slope ζ_{xc}, whose value is suggested to choose from 0.3 to 0.4 for freak waves due to spatio-temporal focusing [7]. When the maximum local wave slope is larger than ζ_{xc}, Eq.(6) is used; otherwise, the p_{sf} is given as zero. They compared the numerical results obtained by using the

modified model with the experimental data using a case with relative small wave height, showing an acceptable agreement. Nevertheless, there are some issues which may be worth of discussing.

One is the definition of U_w^*. The Jeffreys' sheltering theory was originally developed to explain the phase shift of the air pressure and thus modelled the wind effect on the wave growth [12,13]. In this model, the air pressure is related to the relative wind velocity in the frame of fluid motion. For harmonic waves, the wave profile is spatially periodic and travels at the phase velocity and, therefore, the velocity of the wind relative to the wave crests is U_w-c [13]. This justifies Eq. (7) for harmonic waves. However, when it is applied to freak waves or wave groups, one question may be raised, i.e. which phase velocity is suitable to describe the characteristic velocity of the wave group?, since each wave component in the wave group has different phase velocities. Defined by $c_g = \Delta\omega/\Delta k = (\omega_{max} - \omega_{min})/(k_{max} - k_{min})$, where, ω_{max} and ω_{min} are the maximum and minimum frequency of the wave group, respectively, and k_{max} and k_{min} are the corresponding wave numbers, the mean group velocity c_g, on the other hand, represents the wave group propagating speed and has only one value for a wave group. Thus, it is more reasonable and practically easier to choose U_w-c_g to represent the relative velocity between the wind and the fluid than U_w-c.

Secondly, in the modified Jeffreys' theory discussed above, p_{sf} is non-zero only if the maximum local wave slope is larger than the threshold slope ζ_{xc} The numerical investigation by Yan and Ma [8] demonstrates that the modified Jeffreys' theory does not always lead to acceptable results for pressure during the propagation of freak waves. Furthermore, the free surface pressure is not only correlated to the wave slope but also related to the wave elevation, as suggested by Miles [16] and Benjamin [21]. However, the significance of the pressure component related to the wave elevation in the energy transfer from winds to waves strongly depends on the shape of the wave profile. If the wave elevation is symmetrical about the apex point of a crest, e.g. monochromic waves, this pressure component related to the elevation does not cause the energy transfer between the air flow and the waves. In such case, the contribution of the pressure component is neglectable. In the cases for freak waves, the wave profile is usually asymmetrical about the apex point of a crest. The asymmetry sustains during significant period of the propagation of the freak waves. Therefore, the pressure component due to the wave elevation may dramatically affect the energy transfer and so the wave growth. Both the wave slope and the wave elevation need to be taken into account.

Apart from these, other factors, such as vortex shedding and wave breaking, may affect the free surface pressure distribution and cause significant pressure asymmetry with respect to the crest, as revealed in our previous study [8]. The shedding vortex induces a pressure variation at the leeward side of the wave crest and a pressure trough being located near the vortex centre. The magnitude of the pressure trough depends on the vorticity at the centre. When the vortex moves away from the crest, the corresponding pressure variation disappears rapidly. Similarly, the effect of the wave breaking also disappear rapidly after the occurrence of the wave breaking

Based on these, it is suggested here that the air pressure due to the wind be decomposed into two components, i.e. p_{wave} and p_{vor}. The former is closely correlative to the wave slope and wave elevation. The latter is caused by other factors, such as the vortex shedding and wave breaking. Thus, the air pressure may be expressed as

$$p_{sf} = p_{wave} + p_{vor}, \tag{8a}$$

with

$$p_{wave} = \rho_a (U_w - c_g - U_c)^2 (C_a k_c \varsigma + C_b \frac{\partial \varsigma}{\partial x}), \tag{8b}$$

where C_a and C_b are coefficients, whose values need to be determined based on a systematic investigation; k_c is the wave number corresponding to the central frequency of the top-hat wave group used in the paper. For other wave spectrum, e.g. JONSWAP, k_c may be chosen as the wave number corresponding to the significant wave frequency. Eq. (8b) follows Miles' shearing mechanism [14] and Benjamin's theory [21] but is different in two aspects. One is the values of the coefficients C_a and C_b. Because the coefficients in [14] and [21] are based on linear wave theories and suitable for ideal waves, they may not be suitable for the waves with large steepness [23] and/or with strong asymmetric shapes. For the cases with freak waves, the nonlinearity is very strong and the values for the coefficients need to be sought. The second one is the relative speed in bracket, which replaces the reference speed in Miles [14]. In Eq. (8b) the wind driven current U_c is considered in the reference speed. Discussion about it will be given in next section. Inclusion of the current in the definition is only based on the consideration that it is scientifically more reasonable to use U_w-c_g -U_c as the relative velocity between winds and waves than to use U_w-c_g. Nevertheless, the wind-driven current is usually very small compared to the wind, e.g. 3%U_w as suggested in [7], and so including it or not in the definition does not actually make significant difference, as will be demonstrated in Section 4.

3.2. Wind-driven current

As indicated in the Introduction, the wind-driven current needs to be considered when simulating the wind effects on freak waves. In reality, the wind-driven current varies along vertical direction and quickly attenuates to zero with depth. For simplicity, however, similar to Kharif et al [7], a uniform current U_c is assumed to model the effect of the wind-driven current, i.e.,

$$U_c = C_{cur} U_w, \tag{9}$$

where C_{cur} is a coefficient. A detailed investigation on it is presented in this paper to choose a proper value of C_{cur}.

4. Numerical results and discussion

In this section, the wind effects on the change of the freak wave profiles are investigated. For convenience, the parameters with a length scale are nondimensionalised by the water depth d, the time t by $\sqrt{d/g}$ (i.e. nondimensionalised form of the time $\tau = t/\sqrt{d/g}$), the velocity/speed by $\sqrt{gd}$. The vorticity and pressure are nondimensionlised by $|U_w - c_g - U_c|/A_t$ and $\rho_a (U_w - c_g - U_c)^2$, respectively, where A_t is the targeted wave height.

4.1. Freak wave generation

In this paper, the freak waves are generated by the spatio-temporal focusing mechanism, i.e. a sum of a number of sin(cosine) wave components, using a piston-type wavemaker. The displacement of the wavemaker (e.g. [3] and [8]) is given by

$$S(\tau) = \sum_{n=1}^{N} \frac{a_n}{F_n} \cos(\omega_n \tau + \varepsilon_n), \tag{10}$$

where N is the total number of components and $F_n = \dfrac{2[\cosh(2k_n) - 1]}{\sinh(2k_n) + 2k_n}$ is the transfer function of the wavemaker [3]. k_n and ω_n are the wave number and frequency of the n-th component, respectively. They are related to each other by $\omega_n^2 = k_n \tanh(k_n)$. The frequency of the wave components are equally spaced over the range $[\omega_{min}, \omega_{max}]$. ε_n is the phase of the n-th component and is chosen to be $k_n x_f - \omega_n \tau_f$ with x_f and τ_f being the expected focusing point and the focusing time according to linear theory [3]. a_n is the amplitude of n-th

component, which is taken as the same for all components to simplify the relationship between the target amplitude (A_t) of the freak wave and the amplitudes of the components, leading to $a_n=A_t /N$.

In this paper, we focus on freak waves in relatively shallower water and the corresponding study for deep-water cases will be given in future. In this scope, we choose the shortest wave length of wave components is longer than 1(corresponding to the water depth). The corresponding wavelength and *kd* at the central frequency of the wave group used in this study range from 3.10 to 5.62 and from 1.12 to 2.03, respectively.

4.2. Spatial-temporal distribution of the free surface pressure

In order to reveal the feature of the free surface pressure distribution, the numerical approach QALE-FEM/StarCD proposed by the authors of this paper [8] is used. Accuracy investigation of this approach has also confirmed that it can lead to satisfactory results for studying wind effects on 2D freak waves [8]. A range of cases with different freak waves and different wind speeds have been investigated. The spatial-temporal distribution of the free surface pressure and corresponding free surface profiles are recorded. The parameters for these cases are listed in Table 1. According to Yan and Ma [8], the wind effect with wind speed smaller than 0.958 is insignificant. Therefore, the wind speeds in the investigations range from 0.958 to 3.832.

Table 1. Parameters of the cases for 2D freak waves under winds

	ω_{min}	ω_{max}	a_n	τ_f	x_f	c_g	k_c	Wave breaking
Case 1	0.5	1.4	0.008	31.32	10.0	0.597	1.118	Yes
Case 2	0.5	1.4	0.008	46.97	12.5	0.597	1.118	No
Case 3	0.8	1.6	0.00575	46.97	15.0	0.473	1.570	No
Case 4	0.4	1.6	0.007256	39.14	12.5	0.551	1.200	No
Case 5	1.0	1.4	0.006	31.32	12.5	0.482	1.570	Yes
Case 6	0.8	2.0	0.006	46.97	10.0	0.386	2.020	No

Note: N = 32 and the length of the tank is taken as 40 in all the cases.

4.2. 1. Justification of the improved model for air pressure

In Section 2.1, we qualitatively analyse the feature of the free surface pressure due to the wind and suggested an improved model for air pressure (Eq. (8)). In this equation, the air pressure is divided into two components, i.e. p_{wave} and p_{vor}. To evaluate their relative importance, we will fit the free surface pressure using the pressure recorded at the QALE-FEM/StarCD at every time step by

$$p^* = \rho_a (U_w - c_g - U_c)^2 (C_a^* k_c \zeta + C_b^* \frac{\partial \zeta}{\partial x} + p_{ref}), \tag{11}$$

In Eq. (11), p_{ref} is the reference pressure defined in the StarCD package. The coefficients C_a^*, C_b^* and p_{ref} are obtained using a least square method. Considering the fact that, for a focusing wave group, the wave elevation as well as the local wave slope is significant only in a small area, the least square method may not be necessary to perform in the full computational domain but only in a small domain Ω_L near the highest crest or deepest trough at every time step. In this study, it is performed in the sub-domain Ω_L of the computational domain covered by $[x_{peak}- l_l, x_{peak}+l_l]$, in which x_{peak} is the coordinate corresponding to max(|ζ|), i.e. the highest crest or deepest trough at every time step; l_l is a distance reflecting the size of Ω_L and it is taken as $(c_{gmax} - c_{gmin})\tau_f/2$, where c_{gmin} and c_{gmax} are the group velocity corresponding to the wave components with the highest and the lowest frequency, respectively. Numerical investigation indicated that the coefficients C_a^* and C_b^* obtained in this way is not sensitive to the size of the sub-domain $\Omega_{L,}$ as demonstrated in Fig.2, which compares the C_a^* and C_b^* at different time steps in Case 1 listed in Table 1 with different size of the sub-domain Ω_L. Even taking the whole domain, the results are also very close to those with $l_l=(c_{gmax} - c_{gmin})\tau_f/2$. Considering the computational efficiency of the least square method, the $l_l=(c_{gmax} - c_{gmin})\tau_f/2$ is used in this study.

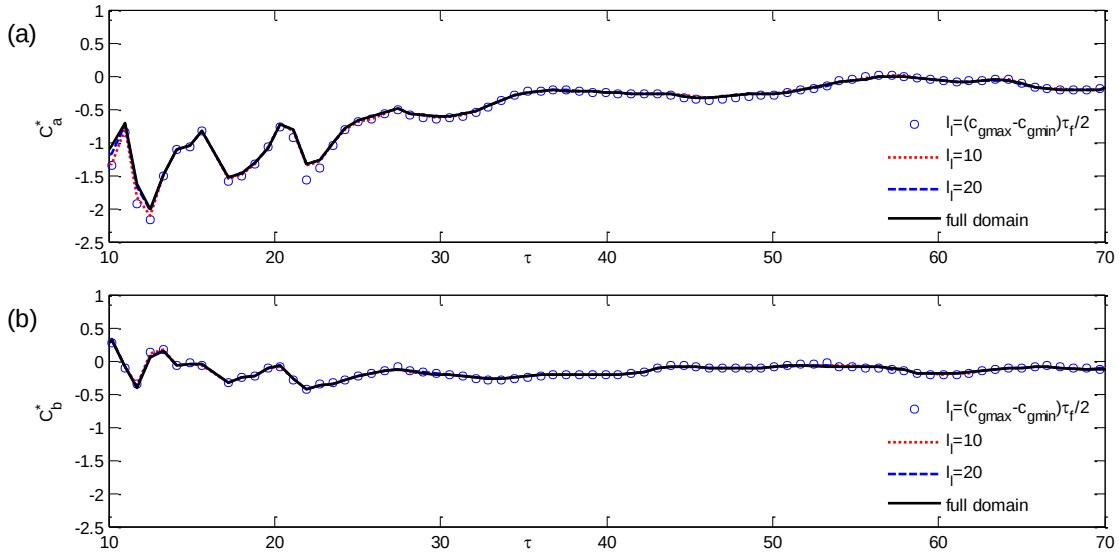

Fig.2 Variation of coefficients C_a^* and C_b^* at different time steps in the cases with different sizes of sub-domain $\Omega_{L,}$ ($\omega_{\min}$ = 0.5 , $\omega_{\max}$ = 1.4, N=32, a_n =0.008, x_f=10, τ_f=31.32, U_w=2.874)

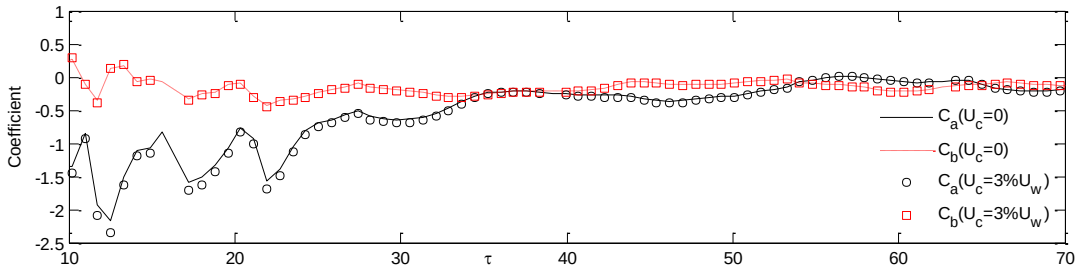

Fig.3 Variation of coefficients C_a^* and C_b^* at different time steps in the cases with different U_c($\omega_{\min}$ = 0.5 , $\omega_{\max}$ = 1.4, N=32, a_n =0.008, x_f=10, τ_f=31.32, U_w=2.874, l_i=(c_{gmax} - c_{gmin})τ_f/2)

In Eq. (11) for the fitting, the value of the wind-driven current U_c will be determined using a series of numerical tests as presented in next section. Considering the fact that U_c is significantly smaller than the wind speed, it has been ignored when performing the least square method for the results shown in Fig.2. However, necessary investigation has been also made to check whether ignoring this term in the fitting process dramatically affects the results of C_a^* and C_b^*. Some results are shown in Fig.3 which compares the variation of coefficients C_a^* and C_b^* at different time steps when different values of U_c are used in fitting process. From this figure, it is observed that the even the U_c is taken as 3%U_w (the wind-driven current as suggested by [7]), C_a^* and C_b^* are very close to those with U_c = 0. This indicates that U_c may not be necessarily considered when estimating C_a^* and C_b^* using Eq. (11) for the fitting. It is worth of noting that U_c is only ignored during the procedure of obtaining coefficients C_a^* and C_b^* when fitting the results obtained by the QALE-FEM/StarCD approach in which the wind-driven current is naturally considered. When using the QALE-FEM combined with the air pressure model to simulate the waves, the wind-driven current needs to be considered, as shown in Fig. 12.

The difference between the pressure calculated using Eq. (11) and those from the QALE-FEM/StarCD calculation should mainly come from the components which is independent of ζ and $\partial\zeta/\partial x$ and corresponding to the term p_{vor}. The difference is measured by a correlation coefficient (R) defined as,

$$R^2 = \frac{\int_{\Omega_L} (p^* - \bar{p})^2 dx}{\int_{\Omega_L} (p - \bar{p})^2 dx}, \tag{12}$$

where p and $\bar{p}$ are the pressure and the average pressure over the entire wave tank, respectively, recorded at the QALE-FEM/StarCD calculation. Smaller correlation coefficient (R) means the difference between the results by Eq. (11) and those from the QALE-FEM/StarCD calculation is larger and thus the components

independent of ζ and $\partial\zeta/\partial x$ are more significant. Therefore, we could evaluate how important the components independent of ζ and $\partial\zeta/\partial x$ are by examining the correlation coefficient. The square of correlation coefficient (R^2) at different time steps corresponding to the results shown in Fig.3 is plotted in Fig.4.

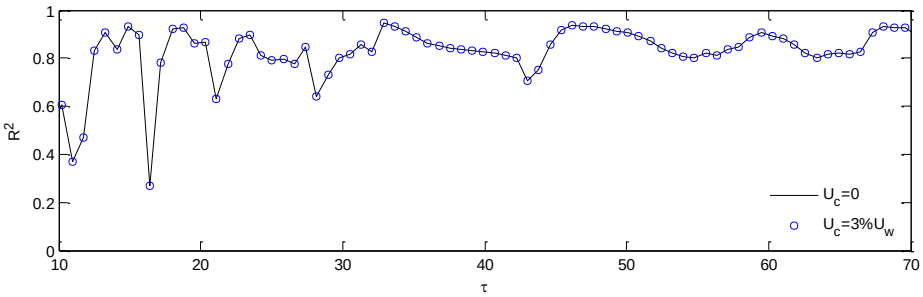

Fig.4 Square of correlation coefficient (R^2) at different time steps ($\omega_{\min}$ = 0.5 , $\omega_{\max}$ = 1.4, N=32, a_n =0.008, x_f=10, τ_f=31.32, U_w=2.874, l_l=(c_{gmax} - c_{gmin})τ_f/2)

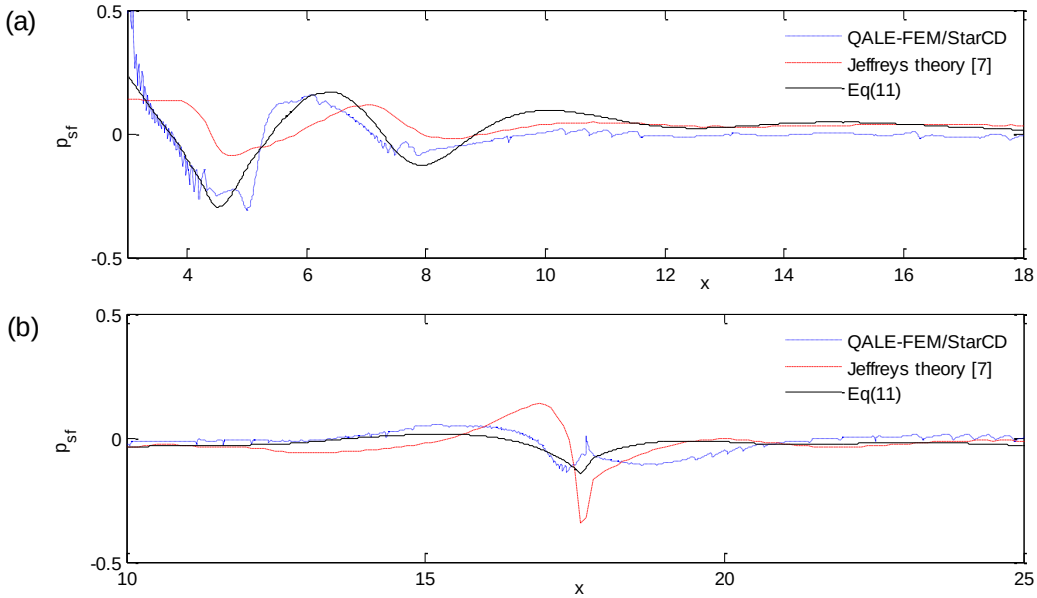

Fig. 5 Comparison of free surface pressure distribution at (a) $\tau \approx 21.91$ (b) $\tau \approx 43.04$ ($\omega_{\min}$ = 0.5 , $\omega_{\max}$ = 1.4, N=32, a_n =0.008, x_f=10, τ_f=31.32, U_w=2.874)

It is found from Fig. 3 that both C_a^* and C_b^* oscillate significantly when $\tau < \tau_f$. During this period, the corresponding correlation coefficient also shows a large oscillation with several low troughs (Fig.4). As discussed above, each low trough of R^2 indicates that there is a significant pressure component independent of ζ and $\partial\zeta/\partial x$. To show how close the results obtained using Eq. (11) and those from the QALE-FEM/StarCD calculation when R^2 is small, the comparisons of the pressure distribution at two time steps are illustrated in Fig.5. For the purpose of comparison, the corresponding results from the modified Jeffreys' theory [7] without applying the threshold slope ζ_{xc} are also plotted together. As observed, Eq. (11) can

reproduce the free surface pressure distribution at those time steps much closer to the QALE-FEM/StarCD than those from the Jeffreys' theory.

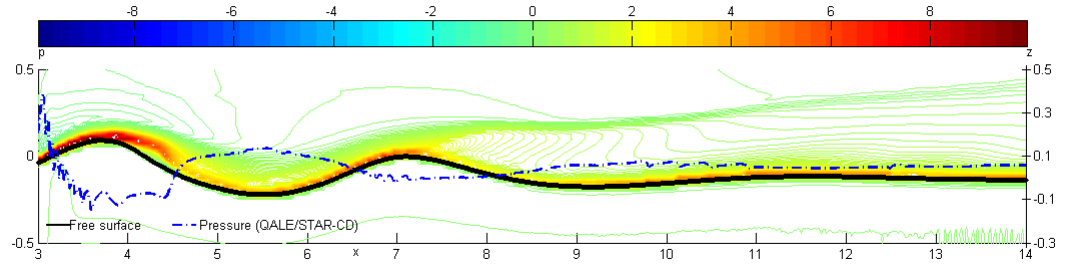

(a) $\tau \approx 21.14$

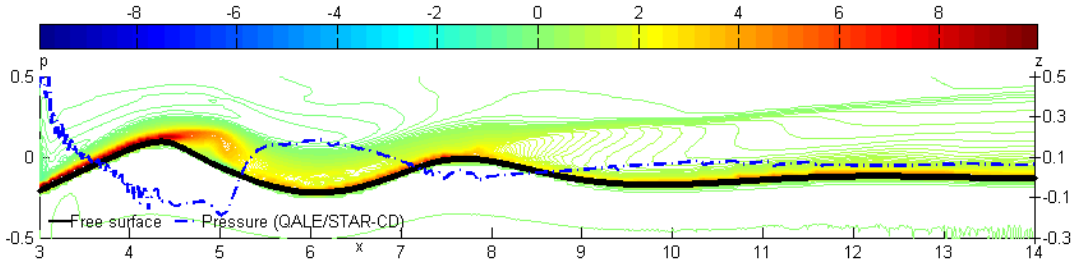

(b) $\tau \approx 21.91$

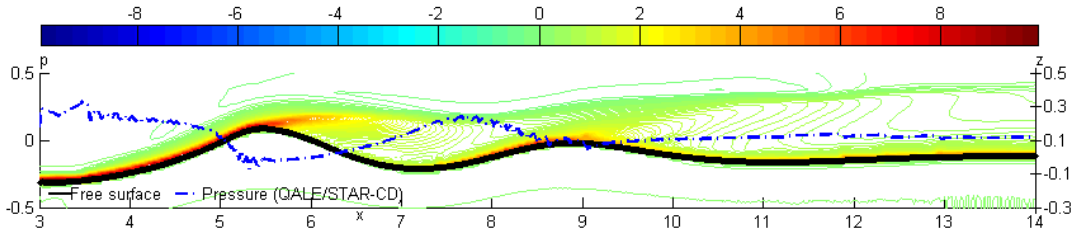

(c) $\tau \approx 23.49$

Fig. 6 Free surface profile, vorticity field and pressure distribution on the free surface near the wave crest at (a) $\tau \approx 21.14$; (b) $\tau \approx 21.91$ and (c) $\tau \approx 23.49$ (U_w=2.874, ω_{min}=0.5, ω_{max}=1.4, x_f=10, τ_f=31.32, N=32) calculated by the QALE-FEM/StarCD approach

In order to find the main reason for what causes the small value of R^2, the free surface profile, vorticity field and pressure distribution on the free surface near the wave crest at different time steps computed by the QALE-FEM/StarCD approach are plotted in Fig. 6. This figure clearly shows that at $\tau \approx 21.14$, a vortex shedding occurs (Fig. 6a). At this moment, the corresponding R^2 reaches a trough value, i.e. 0.6 (Fig. 4). When the shed vortex moves away from the wave crest (Fig. 6b), the vorticity at the centre of the shed vortex decreases. Correspondingly, R^2 increases to about 0.75. At the moment $\tau \approx 23.49$ (Fig. 6c), the vortex almost disappears and the corresponding R^2 reaches a relatively high crest (near $\tau \approx 24$ in Fig. 4). This evidences that the trough of the correlation coefficient around $\tau \approx 20$ in Fig. 4 is mainly caused by the occurrence of the vortex shedding. Similar phenomena are also found for other troughs of the correlation

coefficient in Fig. 4, except that near $\tau \approx 43$. The trough at $\tau \approx 43$ is mainly caused by the wave breaking as shown in Fig. 7. At other time steps without evident vortex shedding and wave breaking, the free surface pressure is closely correlated with ζ and $\partial\zeta / \partial x$, as demonstrated in Fig. 8 which corresponds to R^2=0.83.

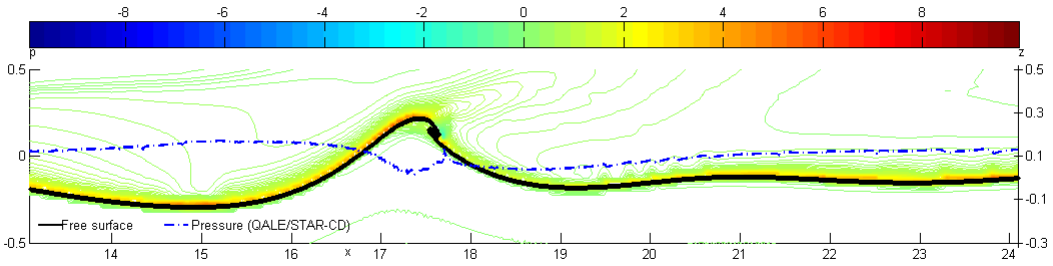

Fig. 7 Free surface profile, vorticity field and pressure distribution on the free surface near the wave crest at $\tau \approx 43.04$ (U_w=2.874, ω_{min}=0.5, ω_{max}=1.4, x_f=10, τ_f=31.32, N=32) calculated by the QALE-FEM/StarCD approach

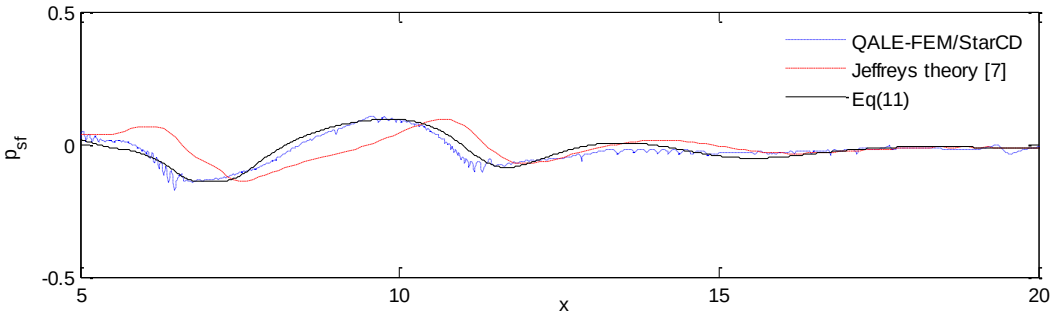

Fig. 8 Comparison of free surface pressure distribution at $\tau \approx 31.32$ ($\omega_{\min}$ = 0.5 , $\omega_{\max}$ = 1.4, N=32, a_n =0.008, x_f=10, τ_f=31.32, U_w=2.874)

All these indicate that the main factors causing the pressure components independent of ζ and $\partial\zeta / \partial x$ are the vortex shedding and the wave breaking. This confirms the justification of Eq. (8) in modelling air pressure for simulating wind effects on freak waves using a FNPT model. It should be noted that when wave overturns and breaking occurs, the free surface becomes a multi-valued function of x, thus Eq. (8) cannot be directly applied. Nevertheless, simulating the wave breaking is beyond the ability of the FNPT model due to the strong viscous effect involved.

4.2. 2. Estimation of p_{wave}

In order to estimate p_{wave} , we need to find the coefficients C_a and C_b . The coefficients C_a and C_b at the time steps involving vortex shedding/wave breaking may be significantly different from those at other time steps. For this reason, we discuss them separately.

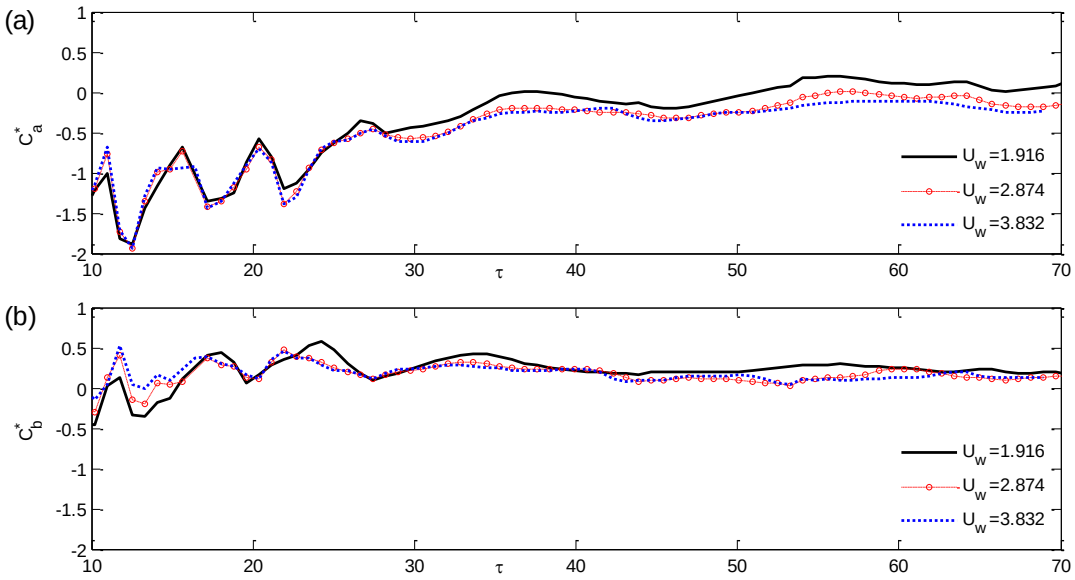

Fig.9 Variation of (a) C_a^* and (b) $C_{b.}^*$ in cases with different wind speeds ($\omega_{\min}$ = 0.5 , $\omega_{\max}$ = 1.4. N=32, a_n =0.008, x_f =10, τ_f =31.32, U_c=0)

At the time steps when the vortex shedding and wave breaking do not occur, e.g. τ ranging from 33 to 40 and τ> 45 in the case shown in Figs. 3 and 4, the effects of vortex shedding and wave breaking may be ignored. In addition, it is also found from Fig. 3 that the coefficients C_a^* and C_b^* oscillate at the early stage i.e. τ <30, and become relatively steady thereafter. This means that when the vortex shedding and wave breaking do not happen, the coefficients C_a^* , C_b^* and so C_a , C_b vary very slowly with time. A similar pattern of the variation of C_a^* and C_b^* at different times is also found in the cases with other wind speeds as shown in Fig.9. This observation indicates that for a specific wind speed, the coefficients C_a and C_b are not significantly affected by the wave profile and, therefore, it is possible to use constant C_a and C_b for the time steps when vortex shedding and/or wave breaking is not significant. On this basis, we suggest use of the following equation to estimate C_a and C_b at the time steps without vortex shedding and/or wave breaking,

$$C_a = \frac{\int_\Gamma C_a^* d\tau}{\int_\Gamma d\tau} \quad \text{and} \quad C_b = \frac{\int_\Gamma C_b^* d\tau}{\int_\Gamma d\tau} \tag{13}$$

in which the integral time domain Γ covers periods when C_a^* and C_b^* vary slowly, excluding those with R^2<0.8. Such definition of the integral time domain may exclude a number of points before the focusing point. However, it doesn't seem to affect the overall results of wind effects on the formation of freak waves as will be presented in following subsections.

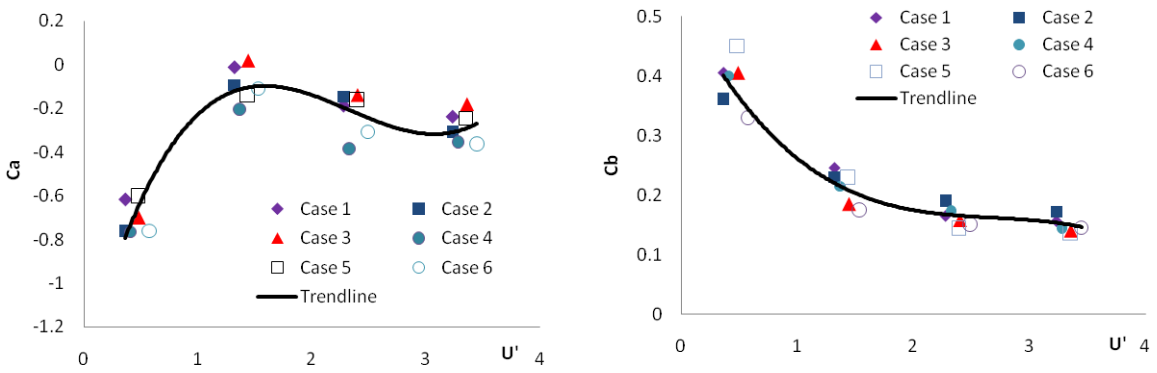

(a) (b)

Fig.10 Characteristic values of (a) C_a and (b) C_b in cases with different freak waves under different winds

To reveal the feature of C_a and C_b given by Eq. (13), all the cases with different wind speeds and different freak waves listed in Table 1 are considered. The corresponding results for C_a and C_b are shown in Fig.10. For convenience, the horizontal axis is taken as $U' = (1 - C_{cur})U_w - c_g$. As can be seen, the results from different cases with the same U' are very close, even though in these cases the frequency structure, focusing time/position and wave amplitude are different and some of them (e.g. Case 1 and Case 5) even involve wave breaking. For C_b, the value consistently decreases as U' increases, while, the value of C_a increases up to $U' \approx 1.5$ and then decreases. Based on figures, third-order polynomial formulas are formed as follows,

$$C_a = 0.1344U'^3 - 0.9394U'^2 + 1.9654U' - 1.3881 \quad (14)$$

$$C_b = -0.0170U'^3 + 0.1369U'^2 - 0.3786U' + 0.5204 \quad (15)$$

It is noted that for small wind speeds, the value of C_b is close to 0.5, the sheltering coefficient taken by Touboul et al [6] and Kharif et al [7]. It is also noted that Eqs (14) and (15) are resulted from the cases listed in Table 1 with the frequency ranging from 0.4 to 2.0 and the wind speed ranging from 0.958 to 3.832. The shortest wave length is longer than the water depth. For the cases with freak waves in deeper water or wind speed being outside of the above range, a further investigation will be carried out in the future.

For the time steps involving vortex shedding and/or wave breaking, it is not easy to find a proper value of C_a and C_b using C_a^* and C_b^*. Nevertheless, one can still use Eq. (8b) with the coefficients determined by Eqs. (14) and (15) to calculate p_{wave} if the resultant error is acceptable.

4.2. 3. Effect of the term p_{vor} on formation of freak waves

As shown in Fig. 3 and Fig. 9, the term p_{vor} in Eq. (8) may dramatically affect the local free surface pressure distribution at the early stage of the freak wave propagation. Its value is not easy to evaluate using a

simple model because it does not only depend on the wave profile but also on the air flow structure above the free surface. In order to investigate the significance of the term p_{vor} on the change of the wave profile, we simulate many cases by using the QALE-FEM method [15, 31], combined with Eq. (8) without considering the effect of p_{vor} i.e. p_{vor} =0. In the simulation, the coefficients C_a and C_b are calculated using Eqs. (14) and (15). We compare the results from the QALE-FEM method with those from the QALE-FEM/StarCD. The results for Case 2 with speed ranging from 0.958 to 3.832 are plotted in Fig. 11, showing the maximum wave height between two consecutive crests and troughs in the wave histories recorded at different positions throughout the tank. The wind-driven current in this figure is chosen as 0.5% U_w . A systematic study on the value of coefficient C_{cur} for the wind driven current will be discussed in the following sub-section.

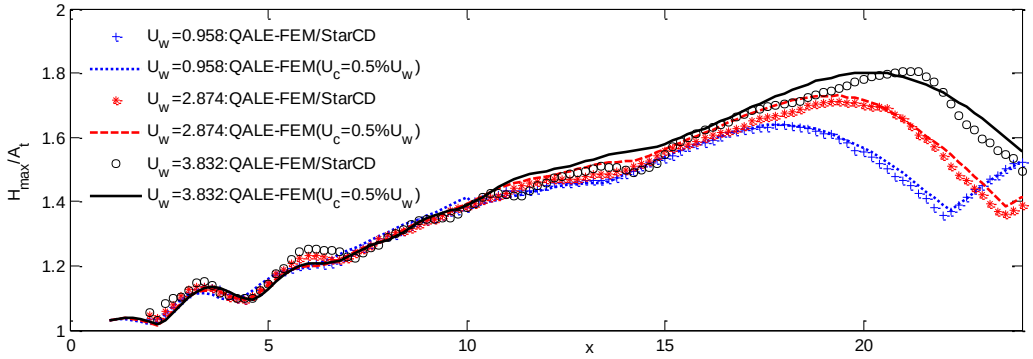

Fig.11 Maximum wave height (H_{max}) recorded at different positions in the cases with different wind speeds ($\omega_{\min}$ = 0.5 , $\omega_{\max}$ = 1.4, N=32, a_n =0.008, x_f=12.4, τ_f=46.97)

From this figure, it is found that the results obtained using the QALE-FEM/StarCD and those from the QALE-FEM coupled by Eq. (8) with p_{vor} = 0 are very close in all the cases considered. This implies that the term p_{vor} may be ignored when predicting the maximum wave height. A similar agreement is also found for other cases without wave breaking in Table 1. A possible reason may be that vortex shedding from the crest sustains only very short period as can be seen from Fig. 4 and Fig. 6; also, the wave group travel fast and therefore the number of shed vortexes is very limited before wave focusing occurs. Based on this, ignoring the effect of p_{vor} is acceptable for predicting the maximum height of the freak waves.

4.3. Overall accuracy of the improved formula

The QALE-FEM is now used to simulate the wind effects on 2D freak waves. By adopting the improved formula, i.e. Eq.(8) with p_{vor} = 0 and the coefficients calculated by Eqs. (14) and (15) , the free surface pressure excited by the winds is modelled. A preliminary accuracy investigation of the improved model for air pressure

has been given in Fig. 11, in which the maximum wave height recorded at different positions along the direction of the freak wave propagation are shown. Apart from the maximum wave height, the maximum wave elevation at different locations may also be important for engineering practice. These results will be examined in this section.

4.3. 1.Wind-driven current and the coefficient C_{cur}

The wind-driven current plays an important role causing the shift of focusing point of the freak waves. As discussed above, the QALE-FEM currently uses a simple model, in which a constant current is introduced using Eq. (9). To ensure the overall effect of this simply model is close to reality, a proper value of C_{cur} needs to be chosen. Fig. 12 shows the maximum elevation recorded at different positions in Case 2 with different wind speeds. Different values of C_{cur} ranging from 0 to 3% have been attempted.

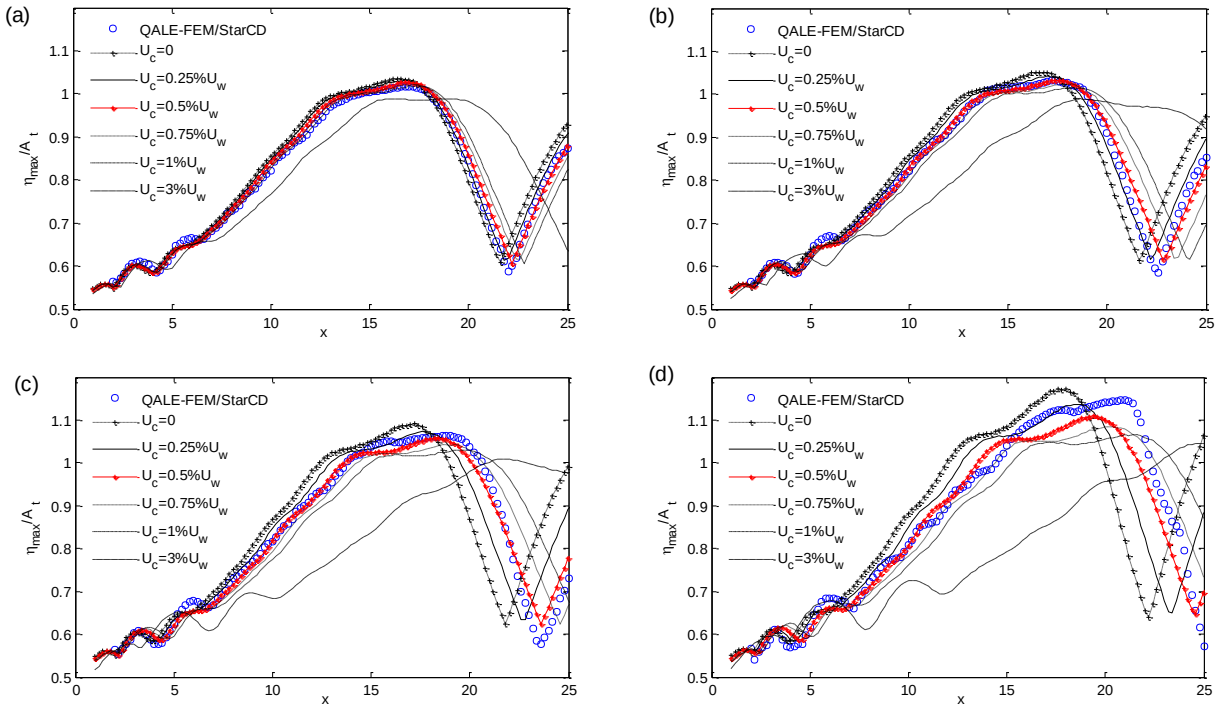

Fig.12Maximum elevation recorded at different positions for (a) U_w= 0.958; (b) U_w= 1.916; (c) U_w= 2.874 and (d) U_w= 3.832 ($\omega_{\min}$ = 0.5 , $\omega_{\max}$ = 1.4, N=32, a_n =0.008, x_f=12.4, τ_f=46.97)

From this figure, it is found that for smaller wind speeds, i.e. U_w= 0.958 (Fig.12a) and U_w= 1.916(Fig.12b), the results with C_{cur} = 0.25% or 0.5% are close to the numerical results from the QALE-FEM/StarCD approach; for the case with U_w= 2.874 (Fig. 12c) , C_{cur} = 0.5% leads to the closest results to the QALE-FEM/StarCD approach; while, for the case with stronger wind, e.g. U_w= 3.832 (Fig.12d), C_{cur} ranging from

0.5% to 0.75% is preferred. One may also find that when C_{cur} = 0.5%, the corresponding results for all wind speeds in Fig. 12 are acceptable. Investigations have also carried out for other cases in Table 1 and similar conclusions have been achieved. Based on this, C_{cur} = 0.5% is used in our investigations below.

4.3. 2.Overall accuracy of the improved formula and comparison with the modified Jeffreys' theory

A further investigation of the improved formulae (Eq. 8(b), Eqs. (14) and (15)) for freak waves with different frequency structures and focusing time/position are also carried out. More results will be presented here. For the purpose of comparison, the modified Jeffreys' model is also adopted by the QALE-FEM. In the simulation using the modified Jeffreys' theory [7], both ζ_{xc} =0.3 and ζ_{xc} =0.4 are tested and the wind-driven current is taken as 0.5%U_w as suggested above.

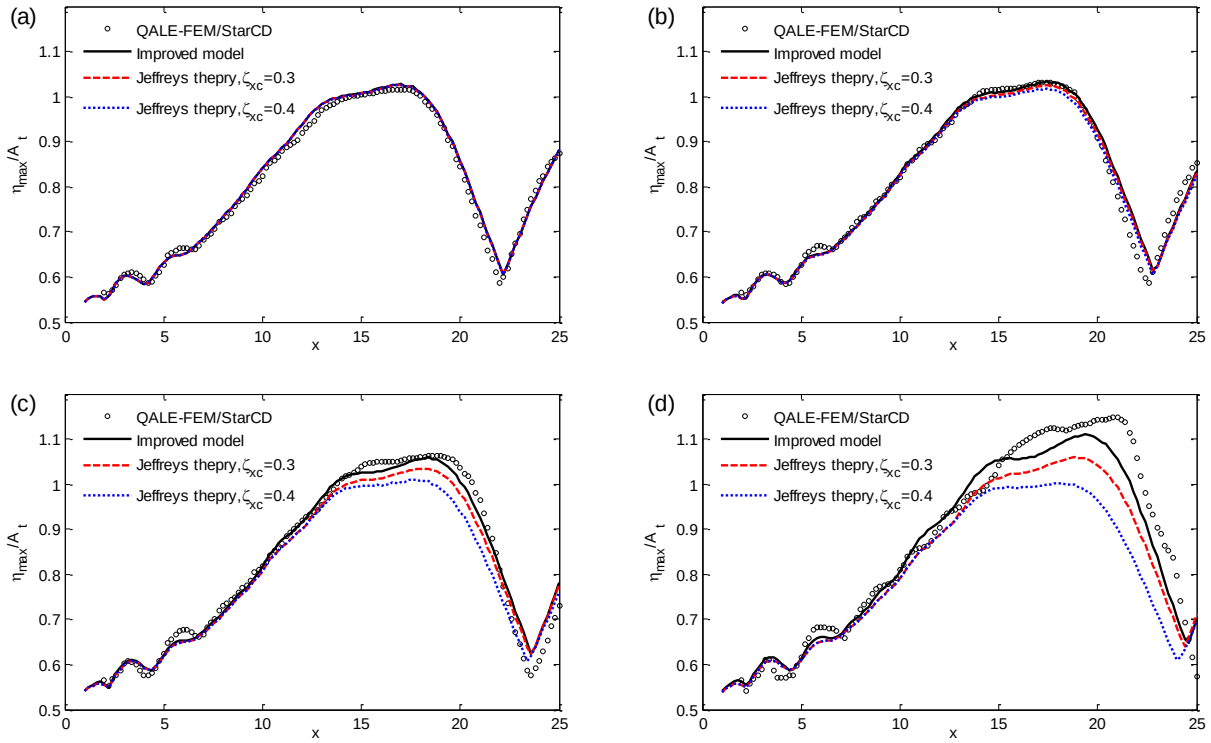

Fig. 13 Comparison of maximum elevation recorded at different positions for (a) U_w= 0.958; (b) U_w= 1.916; (c) U_w= 2.874 and (d) U_w= 3.832 ($\omega_{\min}$ = 0.5 , $\omega_{\max}$ = 1.4, N=32, a_n =0.008, x_f=12.5, τ_f=46.97)

Fig. 13 shows the comparison of the maximum elevations recorded at different position in Case 2. Both the results from the improved model (Eqs. (8), (14) and (15)) and those from the modified Jeffreys' theory [7] are compared with the results obtained by the QALE-FEM/StarCD approach. From this figure, it is observed that for relatively smaller wind speeds, i.e. U_w= 0.958 (Fig. 12a) and U_w= 1.916 (Fig.13b), the improved formula and the modified Jeffreys' theory lead to almost the same results and both are very close to the

results from the QALE-FEM/StarCD approach. For the cases with larger wind speeds, i.e U_w= 2.874 (Fig.13c) and U_w= 3.832 (Fig.13d), the results from the improved formulae are acceptable, but the modified Jeffreys' theory underestimate the maximum elevations no matter which ζ_{xc} is chosen from the range [0.3, 0.4]. The comparison of the maximum elevations is also made for Case 3, in which the frequency structure, wave amplitude and focusing point are different from Case 2. The results are shown in Fig.14. In order to save the space, only the results with U_w= 1.916 and U_w= 2.874 are presented. This figure clearly shows that the improved model leads to much better prediction even at a smaller speed.

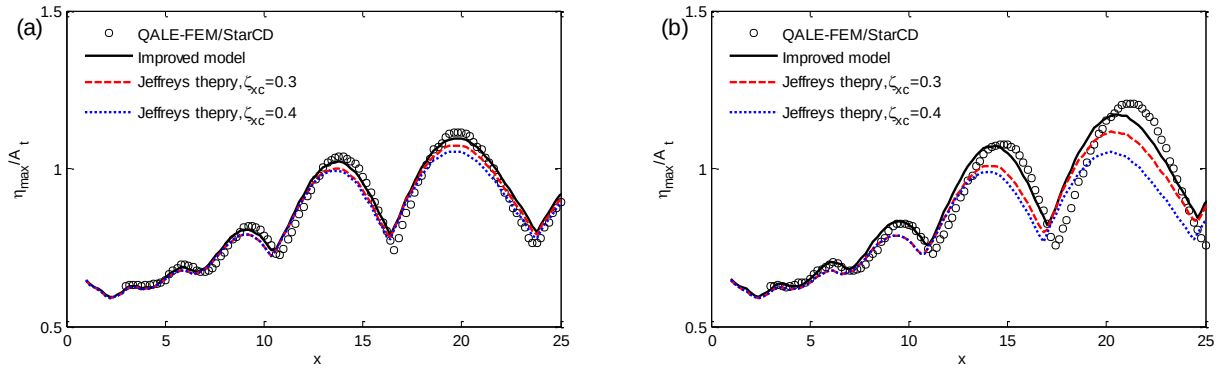

Fig. 14 Comparison of maximum elevation recorded at different positions for (a) U_w= 1.916 and (b) U_w= 2.874 ($\omega_{\min}$ = 0.8 , $\omega_{\max}$ = 1.6, N=32, a_n =0.008, x_f=15.0, τ_f =46.97)

5. Conclusion

In this paper, the features of the pressure distribution over freak waves excited by winds are investigated using the QALE-FEM/StarCD approach, which has been validated in our previous publication. The results show that the pressure does not only depend on the wave slope, but also strongly on the wave elevation. Based on the numerical investigations, an improved model for the air pressure on the free surface for modelling freak waves is suggested, which is given by

$$p_{wave} = \rho_a (U_w - c_g - U_c)^2 (C_a k_c \zeta + C_b \frac{\partial \zeta}{\partial x})$$

$$C_a = 0.1344U'^3 - 0.9394U'^2 + 1.9654U' - 1.3881$$

$$C_b = -0.0170U'^3 + 0.1369U'^2 - 0.3786U' + 0.5204$$

This model can produce acceptable pressure distribution that is very close to that computed by using QALE-FEM/StarCD approach when there is no significant vortex shedding and wave breaking. Although it

may not do so when vortex shedding occurs, overall prediction of freak-wave heights and elevations is much better than the model employed in literature so far, in particular when winds are strong if incorporating the improved model with the full nonlinear potential method – QALE-FEM. This improved model has been tested on the various cases and the results indicate that it is suitable to model freak waves or focusing wave groups with frequency range falling in [0.4, 2.0] under the action of wind with speed ranging from 0.958 to 3.832. Its suitability for the cases in deeper water or the wind speed being outside of the above range needs to be further investigated. In addition, confirmation from experimental results is desired.

Acknowledgement

This work is sponsored by Leverhulme Trust, UK (F/00353/G), for which the authors are most grateful.

Reference

[1] G. Lawton, Monsters of the Deep (The Perfect Wave), *New Scientist*, 170 (2001) 28–32.

[2] C. Kharif, E. Pelinovsky, Physical mechanisms of the rogue wave phenomenon, *Eur J Mech B Fluid*, 22(2003) 603-634.

[3] Q.W. Ma, Numerical Generation of Freak Waves Using MLPG_R and QALE-FEM Methods, *CMES*, 18 (2007) 223-234.

[4] N. Mori, P.C. Liu and T. Yasuda, Analysis of freak wave measurements in the Sea of Japan, *Ocean Eng.*, 29 (2002), 1399-1414.

[5] J.P. Giovanangeli, C. Kharif, E. Pelinovsky, Experimental study of the wind effect on the focusing of transient wave groups, Rogue Wave 2004, Brest, France (http://www.ifremer.fr/web-com/stw2004/rw/)

[6] J. Touboul, J.P. Giovanangeli, C. Kharif, E. Pelinovsky, Freak waves under the action of wind: experiments and simulations, *Eur J Mech B Fluid*, 25 (2006) 662-676.

[7] C. Kharif, J.P. Giovanangeli, J. Touboul, L. Grare, E. Pelnovsky, Influence of wind on extreme wave events: Experimental and numerical approaches, *J. Fluid Mech.* 594 (2008) 209-247

[8] S. Yan, Q.W. Ma, Numerical Simulation of Interaction between Wind and 2-D Freak Waves, *Eur J Mech B Fluid*, doi:10.1016/j.euromechflu.2009.08.001.

[9] S. Yan, Q.W. Ma, Numerical simulation of wind effects on breaking solitary waves, accepted by *19th Int Offshore and Polar Eng. Conf.* (ISOPE), Osaka, 2009.

[10] J. Touboul, C. Kharif, On the interaction of wind and extreme gravity waves due to modulational instability, *Phys Fluid*, 18(2006), 108103

[11] Q.W. Ma, S. Yan, Preliminary simulation on wind effects on 3D freak waves, *Rogue Wave 2008*, Brest, France (http://www.ifremer.fr/web-com/stw2008/rw/)

[12] H. Jeffreys, On the formation of water waves by wind, *Proc. R. Soc. Lond. A*, 107 (1925) 189-206.

[13] H. Jeffreys, On the formation of water waves by wind (second paper), *Proc. R. Soc. Lond. A,* 110(1926) 241–247.

[14] J.W. Miles, On the generation of surface waves by shear flows, *J. Fluid Mech.*, 3 (1957) 185-204.

[15] J.W. Miles, On the generation of surface waves by shear flows, Part 2, *J. Fluid Mech.*, 6 (1959) 568-582.

[16] J.W. Miles, On the generation of surface waves by shear flows, Part 3. Kelvin-Helmholtz instability, *J. Fluid Mech.*, 6 (1959) 583-598.

[17] J.W. Miles, On the generation of surface waves by turbulent shear flows, *J. Fluid Mech.*, 7 (1960) 469-478.

[18] J.W. Miles, Surface-wave generation revisited, *J. Fluid Mech.* 256 (1993) 427-441.

[19] J.W. Miles, Surface-wave generation: a viscoelastic model, *J. Fluid Mech.*, 322(1996) 131-145.

[20] O.M. Phillips, On the generation of waves by turbulent wind, *J. Fluid Mech.* 2 (1957) 417-445.

[21] T.B. Benjamin, Shearing flow over a wavy boundary, *J. Fluid Mech.* 6(1959) 161-205.

[22] S. E. Belcher, J. C. R. Hunt, Turbulent shear flow over slowly moving waves, *J. Fluid Mech.* 251(1993), 109-148.

[23] P.P. Sullivan, J.C. McWilliams, C. Moeng, Simulation of turbulent flow over idealized water waves, *J. Fluid Mech.* 404(2000) 47-85.

[24] T. Yanagi, Costal Oceanography, Series: Ocean Sciences Research, Vol.1, Springer, 1999, 75-81.

[25] J. Touboul, E. Pelinovsky, C. Kharif, Nonlinear Focusing Wave Group on Current, *J. Korean Society of Coastal and Ocean Engineers*, 19(2007), 222~227.

[26] S. Yan, Q.W. Ma, Fully Nonlinear modelling of 2D Freak Waves under Uniform Current, submitted to *J. Comput. Phys.,2010.*

[27] Q.W. Ma, S. Yan, Quasi ALE finite element method for nonlinear water waves, *J. Comput. Phys.*, 212(2006) 52–72.

[28] Q.W. Ma, G.X. Wu, R. Eatock Taylor, Finite element simulation of fully non-linear interaction between vertical cylinders and steep waves. Part 2: Numerical results and validation, *Int. J. Numer. Meth. Fluid*, 36(2001) 287-308.

[29] S. Yan, Q.W. Ma, QALE-FEM for modelling 3D overturning waves, accepted by *Int. J. Numer. Meth. Fluids*, 2009. DOI: 10.1002/fld.2100.

[30] Q.W. Ma, S Yan, QALE-FEM for Numerical Modelling of Nonlinear Interaction between 3D Moored Floating Bodies and Steep Waves, *Int. J. Numer. Meth. Eng.*, 78 (2009), 713-756.

[31] S. Yan, Q.W. Ma, Numerical simulation of fully nonlinear interaction between steep waves and 2D floating bodies using QALE-FEM method, *J. Comput. Phys., 221*(2007), 666-692.

[32] R.G. Dean, R.A. Dalrymple, Water Wave Mechanics for Engineers and Scientists, *World Scientific Publishing Co.*, ISBN 981-02-0420-5,1991